1. Electrochemical Simulation Model

During cell operation, hydrogen and oxygen are transported through the electrode and consumed at the electrode/electrolyte interface (i.e. triple phase boundary) to take part in the electrochemical reactions:

Anode: $$H_2 + O^{2-} \rightarrow H_2O + 2e^-$$ *

MERGEFORMAT (s1)

Cathode: $$\frac{1}{2}O_2 + 2e^- \rightarrow O^{2-}$$ *

MERGEFORMAT (s2)

The balance for a species (e.g. gas and charge species) involved in the electrochemical reaction process in the whole simulation domain, either consumption or production at the TPB, depending on the stoichiometric coefficients v_s, expressed in molar basis as follows:

$$\nabla \cdot N_s = \frac{v_s}{v_e} \cdot \frac{i_0 \lambda^{TPB}}{F} \quad (s = H_2,\ H_2O,\ e^-,\ O^{-2},\ O_2,\ N_2)$$ *

MERGEFORMAT (s3)

where N_s represents the molar flux of the species, v_e the electron transfer number, i_0 the exchange current density per unit length of the TPB, TPB density λ^{TPB} and Faraday constant F.

1.1 Transport in channels

In this study, H_2 is transported from the center bore to the radial micro-channels and permeate transversely through the spongy layer to the reaction sites. The gas flow in this region (i.e., both the center bore and the micro-channels) is governed by continuum physics due to the large size of the micro-channels and the molecule-wall interaction can be safely neglected. Cathode can also treated as a continuum fluid domain [1] as the Knudsen effect is less important compared to the anode due to the larger pore diameter (0.5 to 0.6 μm) [2], larger molecular diameter of O_2 and N_2 (Kn: 0.2 ~ 0.5), higher porosity (0.35) [3] thus less significant concentration overpotential. Both diffusion and convection fluxes are taken into account and represented by the first and second term respectively:

$$N_s = \frac{\rho}{M_s}\left(uw_s - D_o \nabla w_s\right) \quad (s = H_2,\ H_2O,\ O_2,\ N_2)$$ *

MERGEFORMAT (s4)

Where D_o, M_s, w_s, ρ and u represent bulk diffusivity, molecular weight species s, mass fraction of species s, density and velocity of the fluid. The bulk diffusivity in a binary system is calculated as [4, 5]:

$$D_o = \frac{10^{-3} T^{1.75}}{P(V_{s1}^{1/3} + V_{s2}^{1/3})^2}\left\{\frac{1}{M_{s1}} + \frac{1}{M_{s2}}\right\}^{0.5} \quad (s1,\ s2 = H_2 / H_2O \text{ or } O_2 / N_2)$$ *

MERGEFORMAT (s5)

where $V_{s1,s2}$ means the Fuller diffusion volume for the species: H_2 (7.07), O_2 (16.6), N_2 (17.9) and H_2O (12.7).[4] The momentum balance must also be ensured by Navier-Stokes equation with laminar flow condition:

$$\rho(u\cdot\nabla)u=-\nabla P+\nabla\cdot(\mu\nabla u) \quad \backslash^*$$

MERGEFORMAT (s6)

where μ stands for the viscosity.

The viscosity was obtained using Herning and Zipperer method as

$$\mu=\frac{y_{s1}\mu_{s1}\sqrt{M_{s1}}+y_{s2}\mu_{s2}\sqrt{M_{s2}}}{y_{s1}\sqrt{M_{s1}}+y_{s2}\sqrt{M_{s2}}} \quad \backslash^*$$

MERGEFORMAT (s7)

where y_{s1} and y_{s2} represent the mole fraction of species s1 and s2. The species viscosities can be calculated according to Todd and Young [6] as follows:

$$\mu_i=10^{-7}\cdot\sum_{m=0}^{6}b_m\left(\frac{T}{1000}\right)^m \quad \backslash^*$$

MERGEFORMAT (s8)

where b_m represents the factors of the best six-order polynomial fit which describes the dependence of molar heat capacity on temperature.

1.2 Transport in anode spongy layer

Fig. S1 shows the Knudsen number distribution of the H_2 flow at 800 ℃, 1 bar based on the 3D reconstructed pore structure of the spongy layer for BF-S and BF-P. The Knudsen number is calculated by dividing the mean free path with the local pore diameter, which is measured using Local Thickness plug-in in Fiji Software [7]. It is seen that the gas flow in the anode spongy layer is mainly governed by transitional flow physics, so a Knudsen-corrected DGM based on DSMC simulation is used to solve the gas flow for a binary gas mixture:

$$N_{s1}=-\frac{P}{RT}\alpha_{s1}^{-1}\nabla y_{s1}-\frac{y_{s1}}{RT}\left(\alpha_{s1}^{-1}\left(1+\frac{D_{s2,k}^{eff}}{D_o^{eff}}\right)+\frac{kP}{\mu}\right)\nabla P\ \ (s1,\ s2\ =\ H_2,H_2O) \quad \backslash^*$$

MERGEFORMAT (s9)

$$\alpha_{s1}=\frac{1}{D_{s1,k}^{eff}}+\frac{y_{s2}}{D_o^{eff}}\left(1+\frac{y_{s1}}{y_{s2}}\sqrt{\frac{M_{s1}}{M_{s2}}}\right)\ (s1,s2\ =\ H_2,H_2O) \quad \backslash^*$$

MERGEFORMAT (s10)

where *Deff s1,k*, and *Deff o* represent the effective Knudsen diffusivity and the effective bulk diffusivity. *Deff s1,K* and *Deff o* can be obtained by the equations below:

$$D_k^{eff}=\frac{\varepsilon}{\tau_k}D_k \quad \backslash^*$$

MERGEFORMAT (s11)

$$D_k = \frac{d_p}{3}\sqrt{\frac{8RT}{\pi M}} \quad \backslash*$$

MERGEFORMAT (s12)

$$D_o^{eff} = \frac{\varepsilon}{\tau_o} D_o \quad \backslash*$$

MERGEFORMAT (s13)

where τ_o stands for the tortuosity factor of the ordinary flow, which is obtained by the continuum flow simulation in the spongy layer from this study. *k* is obtained by the DSMC simulation which particularly takes the wall slippage effect into account. τ_k thereby *Deff s1,k* is extracted by fitting Eq. * MERGEFORMAT (s9) with the mass flux of H_2 and H_2O from the DSMC simulation.

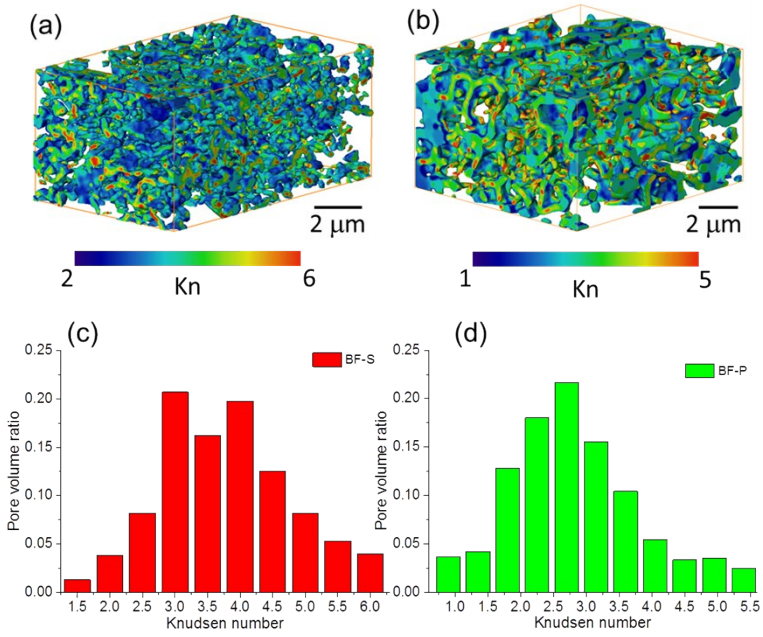

Fig. S1 3D reconstructed pore structure of the spongy layer for (a) BF-S and (b) BF-P, with colour map showing the distribution of Knudsen number of H_2 as a function of the local pore diameter; (c) and (d) quantitative analysis shows that the H_2 flow in spongy layer is within transitional regime.

1.3 Charge transport

The charge transport in the ion conducting phase and electrical conducting phase follows Ohm's law

$$N_s = -\frac{\sigma_p^{eff}}{q_s F}\nabla V_p \quad (s = e, O^{2-}; p = an, ca, ele) \quad \backslash*$$

MERGEFORMAT (s14)

where $\sigma eff\ p$, q_s and V_p represent effective conductivity in the specific phase, species charge and electric potential of phase *p*. The bulk conductivity σ_p is a function of the temperature for each component:[8-10]

$$\sigma_{an} = 3.35\times10^{4}\exp(\frac{-1392}{T}) \quad \backslash*$$

MERGEFORMAT (s15)

$$\sigma_{ca} = 1.23\times10^{4}\exp(\frac{-600}{T}) \quad \backslash*$$

MERGEFORMAT (s16)

$$\sigma_{ele} = \frac{2.5\times10^{7}}{T}\exp(\frac{-9.8\times10^{4}}{RT}) \quad \backslash*$$

MERGEFORMAT (s17)

The effective conductivity is obtained by multiplying the bulk conductivity with the microstructure parameter:[11]

$$\sigma_{p}^{eff} = \frac{\phi_m}{\tau_m}\sigma_p \quad (p = an, ca, ele;\ m = el, io) \quad \backslash*$$

MERGEFORMAT (s18)

where ϕ_m and τ_m indicate the volume fraction and tortuosity factor in phase *p*.

1.4 Reaction kinetics

Butler-Volmer equation is used to relate the generated current density (i_a, i_c) with the local activation overpotential (η_a, η_c) at the anode spongy layer and the whole cathode domain respectively (Eq. * MERGEFORMAT (s19) and Eq. * MERGEFORMAT (s20)). The exchange current density per unit length of the TPB (i_{a0}, i_{c0}, A/m) is coupled with the partial pressure of the reactant and product thereby the mass transport process.[12, 13]

$$i_a = i_{a0}\left\{\exp(\frac{\alpha_a F\eta_a}{RT}) - \exp(\frac{-\beta_a F\eta_a}{RT})\right\} \quad \backslash*$$

MERGEFORMAT (s19)

$$i_c = i_{c0}\left\{\exp(\frac{\alpha_c F\eta_c}{RT}) - \exp(\frac{-\beta_c F\eta_c}{RT})\right\} \quad \backslash*$$

MERGEFORMAT (s20)

$$i_{a0} = i_{a0}^{ref}\exp\{-\frac{E_a^{act}}{R}(\frac{1}{T}-\frac{1}{T_a^{ref}})\}\frac{(\frac{P_{H_2}}{P_{H_2}^*})^{\frac{1-\alpha_a}{2}}(\frac{P_{H_2O}}{1.013\cdot10^5})^{\frac{1+\alpha_a}{2}}}{1+(\frac{P_{H_2}}{P_{H_2}^*})^{0.5}} \quad \backslash*$$

MERGEFORMAT (s21)

$$P_{H_2}^* = \frac{A_{des}\Gamma^2\sqrt{2\pi RTM_{H_2}}}{\gamma_0}\exp(-\frac{E_{des}}{RT}) \quad \backslash*$$

MERGEFORMAT (s22)

$$i_{c0} = i_{c0}^{ref}\exp\{-\frac{E_c^{act}}{R}(\frac{1}{T}-\frac{1}{T_c^{ref}})\}(\frac{P_{O_2}}{P_{O_2}^{ref}})^{0.35} \quad \backslash*$$

MERGEFORMAT (s23)

The local activation overpotential (η_a, η_c) is calculated by subtracting the concentration overpotential ($\eta conc\ a$, $\eta conc\ c$) from the total overpotential as:

$$\eta_a = V_{eq,a} - (V_{ela} - V_{io}) - \eta_a^{conc} = \frac{RT}{2F}\ln(\frac{y_{H_2}}{1-y_{H_2}}) - (V_{ela} - V_{io}) \quad \backslash*$$

MERGEFORMAT (s24)

$$\eta_c = V_{eq,c} - (V_{elc} - V_{io}) - \eta_c^{conc} = E_0 + \frac{RT}{4F}\ln(Py_{O_2}) - (V_{elc} - V_{io}) \quad \backslash*$$

MERGEFORMAT (s25)

where V_{ela}, V_{elc} and V_{io} represent potential of electric conducting phase in anode, cathode and ion conducting phase respectively.

1.5 Boundary conditions and input parameters

The potential at the anode current collector was set to zero and the one at the cathode current collector was set as cell operating voltage V_{cell} as

$$V_{cell} = OCV - V_{pol} \quad \backslash*$$

MERGEFORMAT (s26)

where OCV represents the open circuit voltage and V_{pol} is the polarization of the cell, which was set to sweep from 0 to 1.15 V. The center bore of the anode was fed with H_2 of 99% molar concentration with the flow rate of 30 mL/min. Air was used at the cathode. The input parameters for the developed model are listed in Table S1.

Table S1. Model input parameters for the anode and cathode respectively.

Parameters/Conditions	Value	Unit
Anode	BF-S(BF-P)	
iref a0	4.1×10^{-2} [12]	$A\cdot m^{-1}$
λTPB a	5.3(6.5)	μm^{-2}
E_0	0.98	V
α_a	1.3 [12]	/
β_a	0.7 [12]	/
Eact a	1.2×10^{5} [14]	$J\cdot mol^{-1}$
Tref a	973 [12]	K
A_{des}	5.59×10^{15} [3]	$s\cdot m^2\cdot mol^{-1}$
E_{des}	8.812×10^{4} [3]	$J\cdot mol^{-1}$
Γ	2.6×10^{-5} [3]	$mol\cdot m^{-2}$
ϕ_{el}	0.39 (0.37)	/
ϕ_{io}	0.43 (0.44)	/
ε_{an}	0.17(0.18)	
τ_{el}	4.31	
τ_{io}	2.12	
Cathode		

iref c0	2.5×10^{-4} [1]	$A\cdot m^{-1}$
λTPB c	4.6 [15]	μm^{-2}
α_c	1.5 [1]	
β_c	0.5 [1]	
Eact c	1.4×10^{5} [1]	$J\cdot mol^{-1}$
Tref c	1218 [1]	K
Pref O2	0.21 [1]	atm
ϕ_{el}	0.31	/
ϕ_{io}	0.33	/
ε_{ca}	0.36 [16]	
τ_{el}	31 [15]	
τ_{io}	8.5 [15]	

Table S2. Geometrical parameters of different components (unit: μm)

	Anode channel	Micro-channel (BF-S)	Micro-channel (BF-P)	Spongy layer	Cathode	Electrolyte
L_{length}	100	150	100	200	50	10
L_{width}	400	18	12	400	400	400

2. Gas Permeance Test

Gas flow in the anode substrate with different morphologies was investigated using permeation method at room temperature. Micro-tubular samples were sealed into the system using epoxy resin (Fig. S2) and the flow rates of gas molecules were measured at different feed pressures (0-5 bar). The gas permeance was then calculated using the equation below:

$$\psi = \frac{Q\cdot\ln\left(R_o/R_i\right)}{2\pi L\left(R_o-R_i\right)\Delta P} \qquad \backslash*$$

MERGEFORMAT (s27)

where ψ denotes the gas permeance (mol m^{-2} s^{-1} Pa^{-1}), *L*, *P*, R_o and R_i represent the length (m), pressure (Pa), outer and inner diameters of the tube (m) respectively. *Q* stands for the flow rate (mol s^{-1}).

The gas permeance is a useful means to assess the transport regime as a function of the average pressure $\overline{P} = \left(P_i + P_0\right)/2$. In fact, two extreme scenarios are possible:

1. in continuum regime, the molar flux is dominated by viscous flow, so the gas permeance is proportional to the permeability k_o and to the average gas pressure, as follows[17]:

$$N_{vis} = -\frac{k_o}{\mu}\frac{\overline{P}}{RT}\nabla P \Rightarrow \psi = \frac{k_o}{\mu}\frac{\overline{P}}{RT}\frac{1}{(R_o - R_i)} \quad \backslash*$$

MERGEFORMAT (s28)

2. in Knudsen regime, the molar flux is dominated by Knudsen diffusion, so the gas permeance is proportional to the Knudsen diffusivity while being independent of gas pressure, as follows:[17]

$$N_k = -\frac{D_k^{eff}}{RT}\nabla P \Rightarrow \psi = \frac{D_k^{eff}}{RT}\frac{1}{(R_o - R_i)} \quad \backslash*$$

MERGEFORMAT (s29)

The measured gas permeance is compared with the ones simulated by the I-CFD method, in which the permeability of the spongy region from high resolution scan was simulated by DSMC method with varying pressure gradient (0-3 bar) while the pressure at the outlet was kept constant. The simulated permeability was then used to define the full-thickness anode gas flow simulation, as is shown in Fig. 5. The experiment and simulation results are shown in Fig. S3.

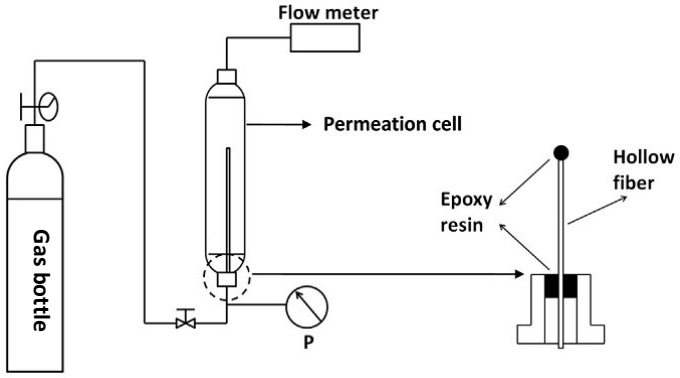

Fig. S2 Schematic diagram of the set-up for gas permeation test

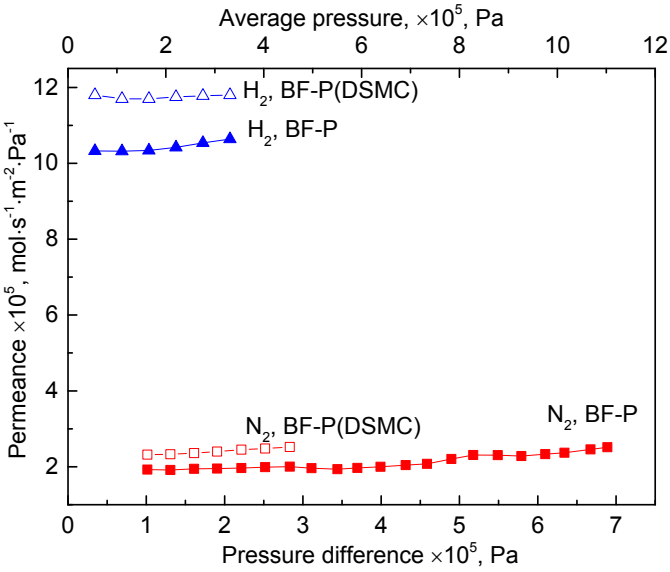

Fig. S3 Comparisons of the gas permeances of BF-P with the I-CFD simulation.

References

1. B. Kenney and K. Karan, *Solid State Ionics*, 2007, **178**, 297-306.
2. Y. Jiang and A. V. Virkar, *Journal of The Electrochemical Society*, 2003, **150**, A942-A951.
3. H. Zhu, R. J. Kee, V. M. Janardhanan, O. Deutschmann and D. G. Goodwin, *Journal of The Electrochemical Society*, 2005, **152**, A2427-A2440.
4. E. N. Fuller, P. D. Schettler and J. C. Giddings, *Industrial & Engineering Chemistry*, 1966, **58**, 18-27.
5. B. Haberman, C. M. Baca and T. Ohrn, *ECS Transactions*, 2011, **35**, 451-464.
6. B. Todd and J. B. Young, *Journal of Power Sources*, 2002, **110**, 186-200.
7. J. Schindelin, I. Arganda-Carreras, E. Frise, V. Kaynig, M. Longair, T. Pietzsch, S. Preibisch, C. Rueden, S. Saalfeld and B. Schmid, *Nat. Methods*, 2012, **9**, 676-682.
8. P.-W. Li and M. K. Chyu, *Journal of Power Sources*, 2003, **124**, 487-498.
9. N. F. Bessette, W. J. Wepfer and J. Winnick, *Journal of the Electrochemical Society*, 1995, **142**, 3792-3800.
10. H. Zhu and R. J. Kee, *Journal of Power Sources*, 2003, **117**, 61-74.
11. H. Iwai, N. Shikazono, T. Matsui, H. Teshima, M. Kishimoto, R. Kishida, D. Hayashi, K. Matsuzaki, D. Kanno, M. Saito, H. Muroyama, K. Eguchi, N. Kasagi and H. Yoshida, *Journal of Power Sources*, 2010, **195**, 955-961.
12. D. G. Goodwin, H. Zhu, A. M. Colclasure and R. J. Kee, *Journal of The Electrochemical Society*, 2009, **156**, B1004-B1021.
13. B. Boer, *SOFC anode: hydrogen oxidation at porous nickel and nickel/zirconia electrodes*, Universiteit Twente, 1998.
14. H. Zhu and R. J. Kee, *Journal of the Electrochemical Society*, 2008, **155**, B715-B729.
15. A. Bertei, J. Mertens and C. Nicolella, *Electrochimica Acta*, 2014, **146**, 151-163.
16. T. Tsai and S. A. Barnett, *Solid State Ionics*, 1997, **93**, 207-217.
17. W. Kast and C. R. Hohenthanner, *International Journal of Heat and Mass Transfer*, 2000, **43**, 807-823.